Energy Procedia 00 (2014) 000–000

Energy Procedia

www.elsevier.com/locate/procedia

SHC 2013, International Conference on Solar Heating and Cooling for Buildings and Industry
September 23-25, 2013, Freiburg, Germany

Collector Simulation Model with Dynamic Incidence Angle Modifier for Anisotropic Diffuse Irradiance

Stefan Hess[a*], Victor I. Hanby[b]

[a]*Fraunhofer Institute for Solar Energy Systems ISE, Heidenhofstrasse 2, 79110 Freiburg, Germany*
[b]*Institute of Energy and Sustainable Development, De Montfort University, Queens Building, The Gateway, Leicester, LE1 9BH, UK*

Abstract

The incidence angle modifier (IAM) of a solar thermal collector for diffuse irradiance is usually determined under the simplifying assumption of isotropic sky and ground radiance. It is applied as one constant collector parameter, independent from slope or weather conditions. The simulation model introduced here considers the varying anisotropy of sky radiance. To create realistic distributions, the approach of Brunger and Hooper is used. Three modes are possible: Mode 1 calculates separate IAMs for anisotropic sky (for every time step) and isotropic ground. Mode 2 calculates separate IAMs for isotropic sky and isotropic ground (once per simulation). Mode 3 uses a user-specified isotropic IAM-value for the collector hemisphere.
The model is applied to a stationary, double-covered process heat flat-plate collector with one-sided CPC booster reflector (RefleC). This collector shows a biaxial and asymmetric IAM for direct irradiance. It is found that, compared to anisotropic modeling, the simplified isotropic model is undervaluing the annual output of this collector by 13.7 % for a constant inlet temperature of 120 °C in Würzburg, Germany. At 40 °C inlet temperature the undervaluation is 9.3 %. For the basis flat-plate without reflector the undervaluation is 7.5 % at 120 °C and 3.3 % at 40 °C. An annual irradiation distribution diagram shows that this is due to an underestimation of diffuse irradiation from directions with high direct irradiation. Detailed results reveal that for RefleC the IAM for anisotropic diffuse sky radiance can vary by up to approx. 25 percentage points during one day.
It is concluded that isotropic modeling of diffuse irradiance can be expected to significantly undervalue the annual output of all non-focusing solar thermal collectors. Highest relevance is found for high collector slopes, complex IAMs and at low-efficiency operation. The optimal collector slope is almost not affected. Accuracy of existing models can be increased by applying Mode 2.

Selection and peer review by the scientific conference committee of SHC 2013 under responsibility of PSE AG.

Keywords: Incidence Angle Modifier (IAM); diffuse radiation; anisotropic sky; collector gain; Brunger model; booster reflector

*Corresponding author. Tel.: +49 (0) 7 61/ 45 88-5739; fax: +49 (0) 7 61/ 45 88-9981.
E-mail address: stefan.hess@ise.fraunhofer.de

Selection and peer review by the scientific conference committee of SHC 2013 under responsibility of PSE AG.

Nomenclature and Abbreviations

	Coefficient of Brunger-model [−]
	Coefficient of Brunger-model [−]
	Coefficient of Brunger-model [−]
	Coefficient of Brunger-model [−]
	Collector heat loss coefficient [W]
	Collector heat loss coefficient [W]
	Thermal capacity of collector [$J\ m^{-2}K^{-1}$]]
	Collector efficiency factor [−]
	Global irradiance on horizontal [$W\ m^{-2}$]
	Extraterrestrial irrad. on horizontal [$W\ m^{-2}$]
	Diffuse irradiance on horizontal [W]
	Beam irradiance on tilted plane [W]
	Diffuse sky irradiance on tilted plane [$W\ m^{-2}$]
	Diffuse ground irradiance on tilted plane [W]
	Diffuse irrad. on tilted plane($G_{st} + G_{rt}$) [W]
	Function within Brunger-model [−
	Fraction of diffuse irradiance on horizontal [−]
	Atmospheric clearness index [−]
	IAM for beam irradiance [−]
	IAM for diffuse irradiance from the sky [−]
	IAM for diffuse irradiance ($G_{st} + G_{rt}$) [−]
	Sky radiance in direction [W]
	Number of steps in direction [−]
	Number of steps in direction [−]
$\dot{q}$	Collector output per aperture area [$W\ m^{-2}$]
	Mean collector fluid temperature [$°C$]
	Ambient temperature [$°C$]

Greek Letters

	Collector slope from horizontal [rad]
	Collector azimuth (west positive) [rad]
	Conversion factor at perpendicular irrad. [−]
	Conversion factor at incidence angle ϑ [−]
	Zenith angle of the sun [rad]
	Zenith angle of sky element [rad]
	Angular width of sky element at θ_h [rad]
	Zenith angle of ground element [rad]
	Angular width of ground elem. at [rad]
	Incidence angle on collector aperture [rad]
	Incidence angle of sun on aperture [rad]
	Incidence angle sky element on ap. [rad]
	Projection of θ into transversal plane [rad]
	Projection of θ into longitudinal plane [rad]
	Effective optical loss factor [−]
	Azimuth angle of sun (west positive) [rad]
	Azimuth sky element (west positive) [rad]
	Angular width of sky element at ϕ_h [rad]
	Azimuth ground element (west pos.) [rad]
	Angular width of ground elem. at ϕ_h^* [rad]
	Angular distance sun to sky element [rad]
	Angular width of sky element [sr]

Abbreviations

CPC	Compound Parabolic Concentrator
IAM	Incidence Angle Modifier

1. Introduction

Non-focusing solar thermal collectors make use of direct and diffuse radiance (cp. Fig. 1). The irradiance varies during day and year with changing sun position and atmospheric conditions. Optical effects of diffuse irradiance are usually calculated isotropic, i.e. with the simplification of homogenous sky radiance. The real sky radiance is to different extents anisotropic, i.e. the spatial irradiance distribution varies due to turbidity, circumsolar radiance and horizontal brightening. Fig. 2 shows a collector with a very distinctive radiation acceptance behavior. It consists of a basis double-covered flat-plate collector and a booster-reflector approximating a one-side CPC-geometry. The specific power output $\dot{q}$ of a solar thermal collector is expressed by eq. 1.

$\dot{q}$ (T) —— *(1)*

Herein, $(\rho\tau\alpha)_{e,\perp}$ is the effective reflectance-transmittance-absorptance product, summarizing all optical losses at perpendicular irradiance. Multiplication with the collector efficiency factor F' gives the conversion factor η_0, i.e. the fraction of perpendicular irradiance converted into useful heat when the mean fluid temperature of the collector T is identical with the ambient temperature T_a. The different irradiation components G_{bt}, G_{st} and G_{rt} are weighted with individual Incidence Angle Modifiers (IAM) K_b, K_s and K_r, to account for changes in the conversion factor due to non-perpendicular irradiance of these radiation components.

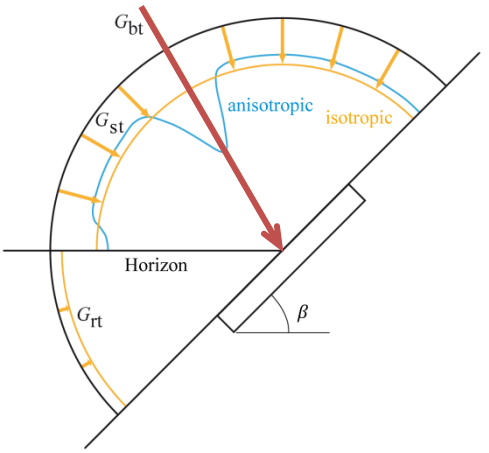

Fig. 1. Components of solar irradiance on a collector with tilt angle β. Beam irradiance G from the sun direction, diffuse irradiance from the sky dome G and reflected diffuse irradiance from the ground reach the collector. For G , the simplifying isotropic and the more realistic anisotropic radiance distribution are indicated.

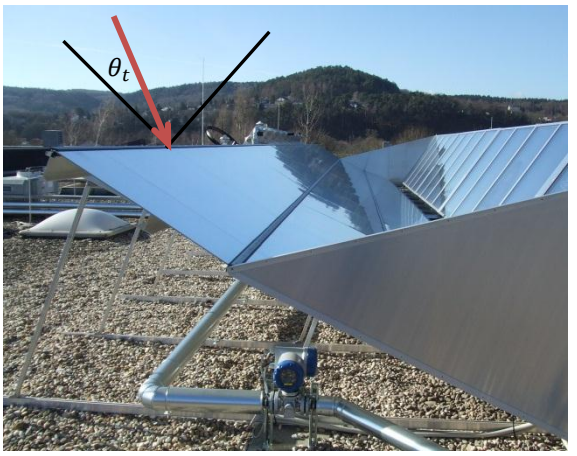

Fig. 2. Low-concentrating, stationary RefleC-collector at the laundry Laguna in Marburg, Germany [1]. The positive transversal incidence angle component θ on the aperture is indicated (cp. Fig 3). The collector trough with concentration ratio 1 26, acceptance half-angle 35° and slope β defines the longitudinal direction.

In eq. 1, the factor c_1 is the collector´s heat loss coefficient at $(T_f - T_a) = 0$. The factor c_2 accounts for the temperature dependence of the heat loss coefficient. The effective thermal capacity c_5 of the collector (all components and fluid content) allows realistic outlet temperature calculation at varying conditions.

Thermally, eq. 1 follows the standard expression of full instantaneous steady state efficiency test results as described in the ISO/FDIS 9806:2013(E) standard [2, p. 109]. For evaluation of dynamic collector tests [2, p. 64] and within most state of the art collector simulations models, G_{st} and G_{rt} are summarized and one single IAM K for diffuse irradiance from the overall collector hemisphere (180°, cp. Fig. 1) accounts for their acceptance (cp. e.g. [3, p. 6]). This K_d is a constant collector parameter determined for isotropic diffuse irradiance and independent of β. It is provided in collector test reports and not varied within a simulation. In eq. 1 and in the model developed, G and G_{rt} are treated separately to allow for separate K_s and K_r.

This work primarily assesses the effect of anisotropic irradiance modeling on the collector output. Therefore, the expression in eq. 1 was considered to be sufficient. Dependencies of the collector efficiency on wind speed and sky temperature, as they are included in the standard dynamic collector model [2, 3, 4], were not taken into account.

The three IAMs of the irradiance components introduced above account for all optical, geometrical and thermal effects occurring when incidence of an irradiance component is not perpendicular to the aperture. The IAM leads to a reduction or increase of η_0, resulting in a parallel translation of the collector efficiency curve. First, in eq. 2, the IAM for beam irradiance K_b is defined [5, p. 297]. The incidence angle θ is projected into the longitudinal and transversal collector planes, where the angles θ_l and θ_t are found (cp. Fig. 3).

(2)

If the factor F' changes with θ, the IAM also accounts for thermal effects. If this is not the case, the right term of eq. 2 is valid and the values for $K_b(\theta_l, \theta_t)$ can be determined by raytracing simulations.

The incidence angle θ on the aperture can be determined by the scalar product of the two unit vectors of collector surface normal and sun direction. The result is shown in eq. 3; it is identical with [5, p. 15]. Fig. 4 shows other relevant angles for the model. Here, also the necessary angular parameters of the Brunger model [6] are indicated.

In principle, for a considered collector distinct values of $K_b(\theta_l, \theta_t)$ could be described by an individual 3D-curve. But assessment of these values by raytracing implies uncertainties and high effort. Thus, in standard collector tests, only values along the characteristic optical axes of a collector are determined.

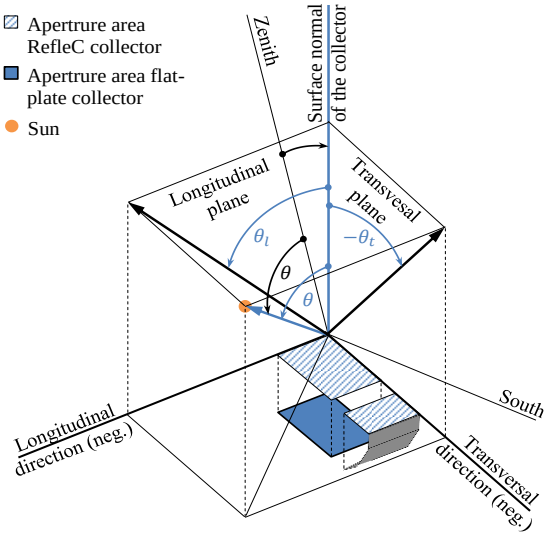

Fig. 3. Reference planes of the RefleC-collector. The longitudinal direction follows the reflector trough (cp. Fig. 2); the transversal direction is perpendicular to it. The incidence angle θ of the sun on the collector is projected into the optical planes and described by θ_l and θ_t. The slope β is found between collector normal and zenith.

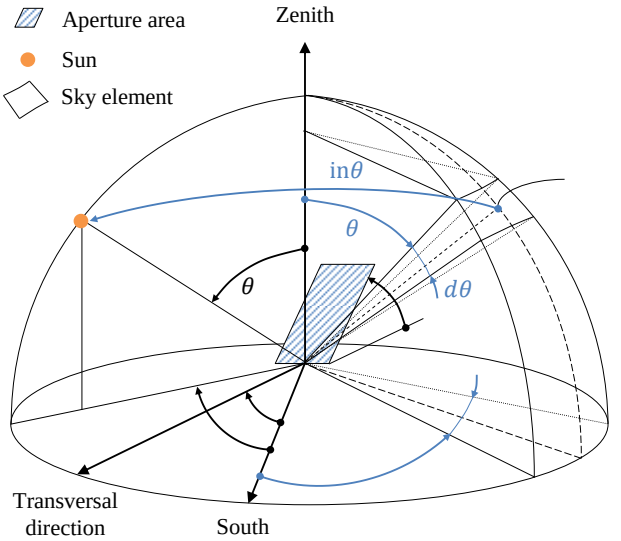

Fig. 4. Horizontal plane with positions of sun and sky element (diffuse radiance). The collector is positioned by azimuth γ and slope β. The sun direction is sun azimuth ϕ_s and solar zenith angle θ_s. The azimuth of the sky element is ϕ_h, its zenith angle is θ_h. The angle between sun position and position of considered sky element is Ψ (cp. [6, p. 55f])

Equations to calculate and have been derived by McIntire and Reed [7, p. 409] and Theunissen and Beckman [8, p. 318]. For RefleC, the scalar product of the adjacent unity vectors (cp. Fig. 3) results in eq. 4 and 5.

As explained, for most directions of beam irradiance on the aperture usually no values of are available. Therefore is in simulations usually approximated according to McIntire [9, p. 315], as in eq. 6.

(3)

n [———————] *(4)*

(5)

≡ *(6)*

Raytracing results for K_b of the RefleC-collector and its basis flat-plate collector without reflector are shown in Fig. 5. It gets obvious that the shape of the -curves along the optical planes highly depends on the collector geometry. For flat-plates, can be approximated to be rotationally symmetrical and described by one single curve (1D-IAM). For evacuated tubes and CPC-collectors, is biaxial symmetrical, i.e. two curves in positive directions $K_b(\theta_l, 0)$ and can be given, since the curves are axially symmetrical (2D-symmetrical-IAM). Because RefleC is not constructed symmetrically in the transversal plane, is described for positive and negative values of θ_l and θ_t (2D-asymmetrical-IAM) as in Fig. 5.

According to Rönnelid et al. [10, p. 285] the approximation of McIntire shows the highest relative errors in K for high incidence angles θ and from directions, where $K_b(\theta_t, 0)$and $K_b(0, \theta_l)$ differ much from each other. This can result in an overestimation of annual energy gain of 4 to 5 % (shown for a CPC).

Siala and Hooper [11, p. 295] have shown the relevance of sky radiance anisotropy for the energy gain of an ideal, symmetrical CPC-collector (acceptance half-angle 36°, inclination = latitude 43.7°). For non-isotropic modeling, the fraction of accepted diffuse irradiance in the course of the day was up to 10 % higher than with an isotropic distribution model.

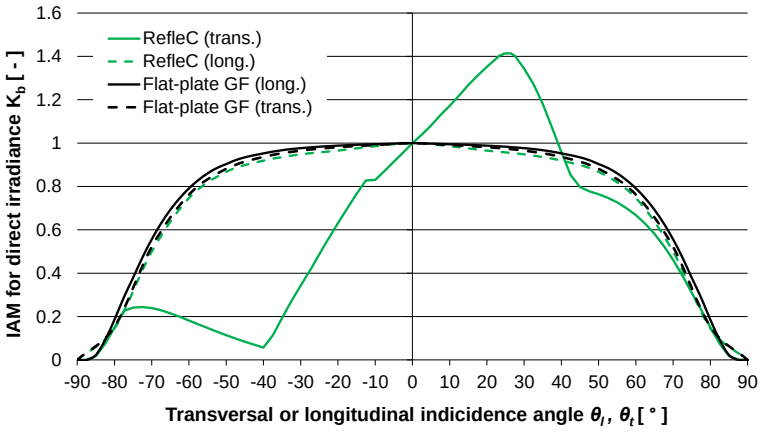

Fig. 5. Raytraced values for) and of the RefleC-collector (2D-asymmetrical-IAM) and its basis flat-plate collector with glass-foil (GF) cover (can be approximated by rotationally-symmetrical 1D-IAM). See Fig. 2 for a picture of the collector(s).

2. Anisotropic Sky Radiance Model of Brunger and Hooper

Within the collector simulation model, the model of Brunger and Hooper [6] is used. It generates a realistic distribution of the sky radiance L at all directions of the sky dome (cp. Fig. 4). Eq. 7 allows a new calculation of the distribution of a given horizontal diffuse irradiance over the hemisphere in every time step.

(7)

The model gives a continuous function for of the sky dome (cp. Fig. 6, 7). Three main fractions of the sky radiance are considered: The coefficient a accounts for the isotropic background; the horizontal brightening is modeled by a cosine-function and the circumsolar radiance is modeled by an exponential function.

In addition to sun position, only the fraction of diffuse irradiance on the horizontal plane G, and the atmospheric clearness index are needed to set up the sky radiance distribution. Brunger and Hooper identified 49 tabulated sets of the coefficients a and a_3. Each set is valid for a certain combination of and k_t (49 radiance distributions), with k and k both separated into nine classes with intervals of 0.1 [6, p. 57].

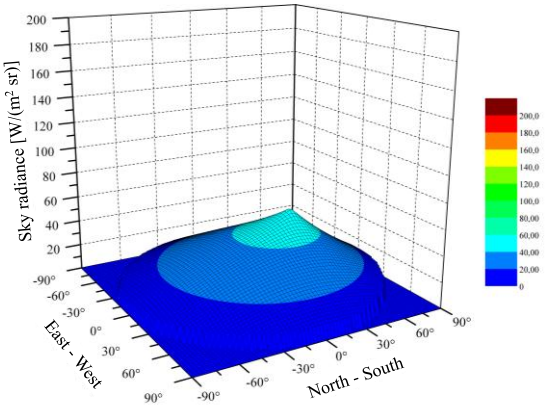

Fig. 6. Brunger-distribution of sky radiance for a **slightly covered sky** ($k = 0.95;\ k_t = 0.35;\ \theta_s = 30°; \phi_s = 0°;\ G_d = 100\ W/m^2$)

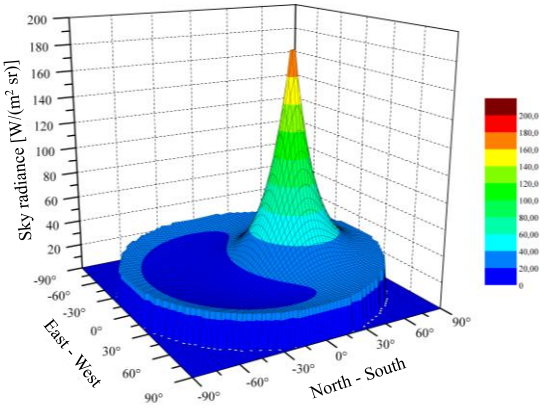

Fig. 7. Brunger-distribution of sky radiance for a **clear sky**

The equations to calculate Ψ, the angular distance between the considered sky element and the sun, as well as $I(\theta_s, a_3)$, a specific function of the Brunger-distribution, can be found in [6, p. 56]. Note that equation $I(\theta_s, a_3)$ contains a typing error in [6, p. 56]. Herein, the first dividend is written as $(1 + exp(-a_3\ \pi/\mathbf{3})$, but must be $(1 + exp(-a_3\ \pi/\mathbf{2})$, (cp. Solar Energy 51/6, Erratum p. 523, 1993). For this work, zenith angle ϕ and azimuth angle θ of a hemispheric segment on the horizontal as identified in [6] were substituted by $\phi_h$and θ_h for a clear distinction from incidence θ on the collector aperture.

Igawa et al. [12] compared different sky radiance distribution models for the whole variety of weather conditions. Among others, they compared their highly elaborated All-Sky-Model-R to the Brunger-model and the Perez All-Weather-Model [13]. With the Brunger-model, the distribution range of predicted around measured values was the highest of all three models but still only 2 $W/(m^2 sr)$ higher than Igawa, when all sky conditions were considered [12, p. 152]. Brunger and Hooper state that their model covers 83 % of the deterministic variation in instantaneous sky radiance and they recommend their model to calculate irradiance incident on CPC collectors with complex or biangular incidence angle modifiers [6, p. 53].

3. Dynamic Collector Simulation Model with Anisotropic IAM calculation

3.1. Approach and Properties

The collector simulation model introduced here was written in FORTRAN and is applied in TRNSYS as user-defined Type 154. Within this Type, the sum of incident G_{st} is distributed over the hemisphere according to the model of Brunger and Hooper (see above). This model was chosen because it creates a realistic and continuous radiance distribution over the hemisphere and it can be set up with relatively low computing effort compared to other models. Type 154 is able to recalculate the IAM K_s for anisotropic sky irradiance for every time step of the simulation. Therefore, the irradiance from each infinitesimal sky element in direction θ_t, θ_l is weighted with the tabulated values of $K_b(\theta_t, \theta_l)$ provided by the user from measurements or raytracing. The model has three modes for the calculation of the IAM for diffuse radiation:

- Mode 1: anisotropic calculation of IAM from sky K_s with Brunger distribution, isotropic calculation of K_r
- Mode 2: isotropic calculation of separate IAM from sky K_s and ground K_r
- Mode 3: manual input of IAM for isotropic diffuse irradiance K_d for whole collector hemisphere (no separation into K_s and K_r). Here, K_d is a collector parameter and independent of β. For $\beta = 0$, K_d equals K_s from Mode 2.

In simulations programs, usually representative weather data files (typical meteorological years) with horizontal radiation data are used. Direct irradiation is measured by pyrheliometers with a solid view angle of approx. 6° aperture diameter with the solar disk in its center [15, p. 49]. Diffuse irradiance on the horizontal is the global irradiance reduced by the pyrheliometer-value [15, p. 49]. In TRNSYS 16, within the weather data processor the simplified Perez diffuse irradiance model for sloped surfaces [16] is the most advanced option to determine G_{st} (Mode 4 in the weather data processor). This model considers the three radiation components isotropic background, circumsolar radiance and horizontal brightening, but does not give a continuous sky radiance distribution. In TRNSYS 17, new fit coefficients for this same model are available [17, p. 7-94f]. Both in TRNSYS 16 and 17 the angular distribution of the sky radiance is not available to the user. This is the reason why the anisotropic sky radiance distribution is calculated within collector Type 154, where it is exclusively used to get a realistic value of K_s. The value of G_{st} is still taken from the weather data processor.

3.2. Beam Irradiance

The incidence angle for beam irradiance and its components are calculated with eq. 3 to 5. $K_b(\theta_t, \theta_l)$ is then interpolated from the values provided by the user in an external table. These values can be raytracing data for the whole collector hemisphere (exact values from 3D-raytracing) or can be generated from measurements along the collector axis and by using eq. 6. Thus, terrors by applying the separation approach of McIntire [9] are not made within Type 154 and could be avoided by providing values for $K_b(\theta_t, \theta_l)$ from the whole collector hemisphere.

3.3. Anisotropic Sky Irradiance

The calculation of the IAM for diffuse irradiance from the sky K_s is shown in eq. 7 to 9. Eq. 7 is based on the fundamental approach of Brandemuehl and Beckman for calculation of effective incidence angles [18, p. 511]. The sky radiance $L(\theta_h, \phi_h)$ of an infinitesimal sky element $d\Omega$ is located by its angle θ_h from the zenith and its azimuth angle ϕ_h (cp. Fig. 4). The incidence angle of $d\Omega$ on the collector is $\theta(\theta_h, \phi_h)$. The absorbed diffuse irradiance from the whole sky in the numerator is the integral of the irradiance of all sky elements $d\Omega$ weighted with their individual IAM $K_b(\theta_h, \phi_h)$ and their individual cosine losses ($\cos\theta(\theta_h, \phi_h)$). Division by the overall sky diffuse irradiance on the aperture gives the IAM for anisotropic diffuse irradiance.

$$K_s = \frac{\int_{\frown} K_b(\theta_h, \phi_h) \cdot L\,(\theta_h, \phi_h) \cdot \cos\theta(\theta_h, \phi_h)\, d\Omega}{\int_{\frown} L\,(\theta_h, \phi_h) \cdot \cos\theta(\theta_h, \phi_h)\, d\Omega} \qquad \text{with } d\Omega = \sin\theta_h\, d\theta_h\, d\phi_h\,; \quad \text{for } \theta\ [0; 90°] \tag{7}$$

$$K_s = \frac{\int_0^{2\pi} \int_0^{\frac{\pi}{2}} K_b\big(\theta_t(\theta_h, \phi_h), \theta_l(\theta_h, \phi_h)\big) \cdot L\,(\theta_h, \phi_h) \cdot \cos\theta(\theta_h, \phi_h) \cdot \sin\theta_h\, d\theta_h\, d\phi_h}{\int_0^{2\pi} \int_0^{\frac{\pi}{2}} L\,(\theta_h, \phi_h) \cdot \cos\theta(\theta_h, \phi_h) \cdot \sin\theta_h\, d\theta_h\, d\phi_h} \qquad \text{for } \theta\ [0; 90°] \tag{8}$$

The incidence angle $\theta(\theta_h, \phi_h)$ of $d\Omega$ on the collector aperture in eq. 8 as well as $\theta_t(\theta_h, \phi_h)$ and $\theta_l\,(\theta_h, \phi_h)$ can be calculated by eq. 3 to 5, since the coordinates of the sun (θ_s, ϕ_s) and of $d\Omega\ (\theta_h, \phi_h)$ have the same horizontal basis (zenith and south direction). The width of $d\Omega$ increases with $\sin\theta_h$(cp. Fig 4). The computable equation is:

$$K_s = \frac{\sum_{i=0}^{n_{\phi_h}} \sum_{j=1}^{n_{\theta_h}} K_b\big(\theta_{t,ij}, \theta_{l,ij}\big) \cdot L_{ij}\big(\theta_{h,ij}, \phi_{h,ij}\big) \cdot \cos\theta_{ij}\big(\theta_{h,ij}, \phi_{h,ij}\big) \cdot \sin\theta_{h,ij} \Delta\theta_h \Delta\phi_h}{\sum_{i=0}^{n_{\phi_h}} \sum_{j=1}^{n_{\theta_h}} L_{ij}\big(\theta_{h,ij}, \phi_{h,ij}\big) \cdot \cos\theta_{ij}\big(\theta_{h,ij}, \phi_{h,ij}\big) \cdot \sin\theta_{h,ij} \Delta\theta_h \Delta\phi_h} \qquad \text{for } \theta_{ij}[0; 90°] \tag{9}$$

In Type 154, $\Delta\theta_h$ and $\Delta\phi_h$ can be selected as model parameters. For width of $\Delta\theta_h = \Delta\phi_h = 5°$ the numerical integration to receive K_s by simulation needs 1296 loops per time step (18 steps in direction θ_h and 72 in direction ϕ_h) for the numerator and the denominator respectively. This is highly increasing the simulation time, so angular width and time step must be chosen reasonably. The denominator in eq. 9 gives G_{st} calculated with the Brunger model, but this is only an informative value and not used in eq. 1.

3.4. Isotropic Sky and Ground Irradiance

For the assumption of isotropic diffuse irradiance, Carvalho et al. [19] presented integration limits to calculate K_s and K_r of collectors with 1D and 2D symmetric IAM. This can be very useful when an analytic solution of the integration can be derived for a certain collector. In case of numerical integration, the integration limits of K_s and K_r depend on β only, since the integration can be restricted to $\theta\ [0; 90°]$, as it is done in eq. 7 to 9. Within Type 154, K_s for isotropic sky radiance is computed numerically based on the horizontal plane just as in eq. 9. For this case of isotropic radiance, $L_{ij}\big(\theta_{h,ij}, \phi_{h,ij}\big)$ can be omitted. The equation is independent of β and valid for all possible IAM-shapes. Since only sky radiance from $\theta_{h,ij}$ and $\phi_{h,ij}$ within $\theta_{ij}[0; 90°]$ is considered, eq. 9 does not have to be further modified. The integration widths are set to fixed values $\Delta\theta_h = \Delta\phi_h = 2.5°$.

For computing K_r with the approach of eq. 9, the calculation cannot be based on the horizontal plane anymore, since for zenith angles above 90° numerical problems occur for incidence angle calculation. Thus, the integration is performed based on the collector plane and new zenith and azimuth coordinates for diffuse irradiance from the ground with certain integration limits are used. The zenith angle θ_h^* [0; 90°] and the azimuth angle ϕ_h^* [−90°; +90°] of reflected irradiance are based on the collector plane with slope β from horizontal. The orientation of zenith and azimuth is the same as in Fig. 4. For the numerical integration, the angular width is set to $\Delta\phi_h^* = 2.5°$ (72 segments) and $\Delta\theta_h^* = \beta/36$ (maximum 2.5° for $\beta = 90°$). The longitudinal and transversal incidence angles of the reflected irradiance can be calculated with eq. 4 and 5 when omitting γ and β.

4. Application to a Low-Concentrating, Stationary Process Heat Collector

Fig. 8 illustrates the effects of anisotropic modeling of K_s by use of Type 154. To calculate K_{dt}, the the K_b-values of RefleC given in Fig. 5 are used (from an input-File containing values of $K_b(\theta_l, \theta_t)$ generated by the separation approach of McIntire (cp. section 1 and [7]). At solar noon, $K_b$reaches values close to 1.4, since at this time of the year around summer solstice $\theta_t \approx +30°$ onto the aperture is reached for $\beta = 55°$.

In diffuse Mode 3, the isotropic IAM for the whole collector hemisphere K_d is also calculated based on the data in the input-file. The integration results for K_s and K_r are highly differing from K_d because of the very incidence angle selective behavior of RefleC in the transversal direction (cp. Fig. 5).

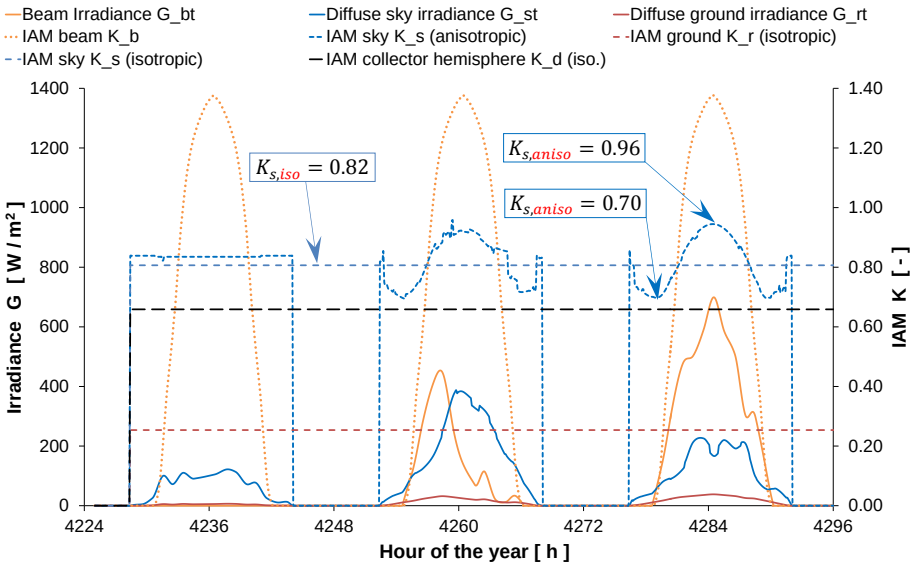

Fig. 8. IAM values for the different irradiance components on a RefleC collector with $\beta = 55°$ and $\gamma = 0°$ in Würzburg. Three characteristic days in June (day 177-179) are shown. If the hemispheric isotropic Mode 3 is selected, the sum $G_{dt} = G_{st} + G_{rt}$ is weighted with $K_d = 0.66$. In Mode 2, separate and β-dependent but still constant isotropic IAMs $K_{s,iso} = 0.82$ and $K_r = 0.25$ are calculated. Only the values of $K_{s,aniso}$ calculated in Mode 1 response to the actual irradiance conditions based on a new Brunger-distribution for every time step (5 min).

On the first day shown, the weather data file does not contain any beam irradiance at all, so the diffuse fraction k is maximal. Since a significant amount of diffuse irradiance is observed, the clearness index k_t is low but not at its minimum. Thus, a slightly covered sky as in Fig. 6 is assumed and $K_{s,aniso} = 0.84$ is slightly higher than $K_{s,iso}$ but does not change significantly during the day. The third day in contrary is very sunny with either a clear or partly cloudy sky (cp. Fig. 7). These conditions cause a high anisotropy of the diffuse irradiance on the aperture. In the morning after sunrise, solar disk and thus circumsolar radiance are behind the collector (i.e. $\theta > 90°$). The majority of diffuse sky radiance is in the northern hemisphere, so for the RefleC-aperture, $K_{s,aniso}$ is smaller as for the isotropic assumption. With progressing sun movement in the course of the day this changes, and around noon the circumsolar radiance is incident at $\theta_t \approx +30°$, where the acceptance of RefleC is optimal. Fig. 9 shows that $K_{s,aniso}$ can change by up to approx. 25 %-points during one day. Qualitatively very similar daily variations of $K_{s,aniso}$ like in the days two and three shown are also predicted by Siala and Hooper [11, p. 295].

Since the transversal IAM $K_b(0, \theta_t)$ is highly relevant for the annual energy gain of the stationary RefleC-collector, the distribution of irradiation (sum of irradiance during the course of the year) within the transversal plane is decisive for the collector energy gain. The influence of the anisotropy of diffuse irradiance on this distribution is illustrated in Fig. 9. When the anisotropy of $G_{st}$is considered, less diffuse irradiance occurs from northern directions. A significant increase of diffuse irradiation is observed in the range of $\theta_t[-5°;\ 35°]$. At these incidence angles, the highest IAM-values $K_b(0, \theta_t)$ occur, so that a significant influence on the annual energy gain can be expected.

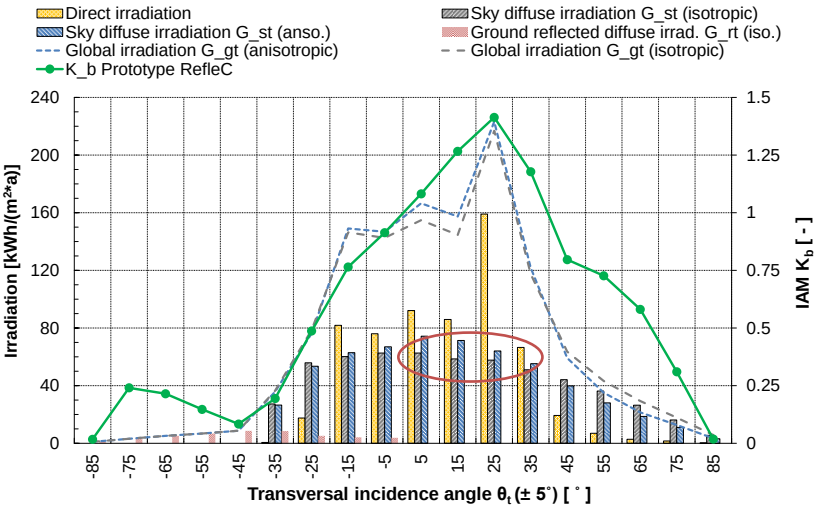

Fig. 9. Annual irradiation distribution diagram for 10°-slices of the hemisphere for an aperture with $\beta = 55°$ and $\gamma = 0°$ in Würzburg, Germany. The global irradiation on the tilted plane is 1213 kWh/(m^{2}a); the diffuse fraction is 50 %. Contrary to Rönnelid et al. [10] all cosine-losses in longitudinal and transversal direction are considered. The irradiance on the tilted plane was calculated with the Perez-Model in the weather data reader of TRNSYS. Mean IAM-values $K_b(0, \vartheta_t)$ of RefleC (cp. Fig. 3) are indicated for each interval (cp. Fig. 5).

The influence of the anisotropy of solar irradiance on the annual energy gain of RefleC has been investigated in TRNSYS using Type 154 described above. The results of this study are shown in Tab. 1.

Tab. 1. Annual energy gain of RefleC and its basis flat-plate for anisotropic sky radiance at different locations and inlet temperatures T_{in}. The collectors were simulated according to eq. 1 with their real thermal capacities at a constant mass flow of 25 l/m^2_{Ap}. The efficiency curves have been determined at the Test Lab Solar Thermal Systems at Fraunhofer ISE for mean fluid temperatures up to $T_m = 163\ °C$(RefleC) and $T_m = 138\ °C$ (flat-plate). No system or connection losses were considered, every positive temperature lift was counted. Results are given for optimal collector slope, ground albedo of 0.2 and a simulation time step of 15 min. The undervaluation of the described annual gain is given for isotropic modeling of diffuse irradiance. The irradiance on the tilted plane was calculated with the Perez-Model in TRNSYS 16. In Würzburg, at $\beta = 55°$ the fraction of diffuse irradiation is 50 % (sky: 46 %, ground 4 %), for Seville at $\beta = 45°$ it is 36 % (sky: 33 %, ground 3 %).

	Würzburg (RefleC: $\beta = 55°$; flat-plate: $\beta = 37.5°$)			**Seville** (RefleC: $\beta = 45°$; flat-plate: $\beta = 37.5°$)		
Collector type and inlet temperature T_{in}	Collector gain Mode 1 [a] (kWh m^{-2}a^{-1})	Mode 2 undervaluation [b]	Mode 3 undervaluation	Collector gain Mode 1 (kWh m^{-2}a^{-1})	Mode 2 undervaluation	Mode 3 undervaluation
RefleC						
40 °C	771	-2.8 %	- 9.3 %	1397	- 1.6 %	- 3.8 %
120 °C	271	-6.5 %	**- 13.7 %**	**638**	- 3.8 %	- 6.4 %
Flat-plate [c]						
40 °C	645	-1.6 %	**- 3.3 %**	1195	- 0.9 %	- 1.7 %
120 °C	145	-5 %	- 7.5 %	**415**	- 2.7 %	**- 3.9 %**
Increase [d]						
40 °C	+19.6 %	+18.1 %	+12.2 %	+17.0 %	+16.2 %	+14.5 %
120 °C	**+87.0 %**	+84.0 %	**+74.4 %**	+53.7 %	+51.9 %	+49.7 %

[a] Mode 1: anisotropic sky, isotropic ground; Mode 2: isotropic sky, isotropic ground; Mode 3: isotropic collector hemisphere (1 IAM for diffuse irradiance from sky and ground as usually applied)
[b] Undervaluation of collector gain compared to Mode 1
[c] Basis flat-plate collector of RefleC (without reflector) with glass-foil double cover
[d] Increase of annual collector output due to reflector per m^2 Aperture of basis flat-plate collector

5. Conclusions and Outlook

A modeling approach to consider the anisotropy of sky radiance has been introduced. It has been applied to a solar thermal collector with an approx. rotationally symmetric IAM and to a collector with an asymmetric, biaxial IAM-curve. The sky anisotropy was found to be most relevant for the latter, for low efficiency operation (high temperatures) in general, and for realistic dynamic behavior. For locations with higher diffuse fractions, the sky radiance anisotropy is assessed to be relevant also for standard collectors at standard application temperatures.

To increase the accuracy of standard simulation tools, a change from modeling Mode 3 to Mode 2 should be considered. K_s and K_r for isotropic irradiance are being calculated only once, so simulation time is not affected. The detailed Mode 1 highly increases simulation time. For some collector types like symmetric CPC-collectors the undervaluation of diffuse acceptance might be partly compensated by an overvaluation due to the separation approach of McIntire. With Mode 1 this can be assessed for the different collector types, since three-dimensional IAM curves from raytracing can be read without further increase of simulation time.

The predicted output has to be compared with measured collector output. Also, the simplified simulation of the collector gain (constant mass flow, every positive efficiency counted) has to be compared with realistic operation.

Acknowledgements

We are very thankful for the support of Wagner & Co. Solartechik GmbH, the German Ministry for the Environment, Nature Conservation and Nuclear Safety (BMU) and the Reiner Lemoine Foundation.

References

[1] Hess, S., Oliva, A., et al. (2010). Solar Heat for Industrial Processes: RefleC-Collector Development and System Design. EuroSun 2010.
[2] ISO/FDIS 9806:2013(E). Solar energy - Solar thermal collectors - Test methods. NA 041-01-56 AA - SpA CEN/TC 312 and ISO/TC 180. Final Draft by International Organization for Standardization (ISO) and European Committee for Standardization (CEN), Brussels.
[3] Haller, M., Perers, B., et al. (2013). TRNSYS Type 832 v5.01: Dynamic Collector Model by Bengt Perers - Updated Input-Output Reference. URL: http://www.solarenergy.ch/Type-832-Kollektormodell.223.0.html?&no_cache=1&L=0&no_cache=1.
[4] Fischer, S., Heidemann, W., et al. (2004). Collector test method under quasi-dynamic conditions according to the European Standard EN 12975-2. Solar Energy 76(1–3): 117-123.
[5] Duffie, J. A. and Beckman, W. A. (2006). Solar Engineering of Thermal Processes. 3rd Edition. New Jersey, John Wiley & Sons, inc.
[6] Brunger, A. P. and Hooper, F. C. (1993). Anisotropic sky radiance model based on narrow field of view measurements of shortwave radiance. Solar Energy 51(1): 53-64.
[7] McIntire, W. R. and Reed, K. A. (1983). Orientational relationships for optically non-symmetric solar collectors. Solar Energy 31(4): 405-410.
[8] Theunissen, P. H. and Beckman, W. A. (1985). Solar transmittance characteristics of evacuated tubular collectors with diffuse back reflectors. Solar Energy 35(4): 311-320.
[9] McIntire, W. R. (1982). Factored approximations for biaxial incident angle modifiers. Solar Energy 29(4): 315-322.
[10] Rönnelid, M. and Karlsson, B. (1997). Irradiation distribution diagrams and their use for estimating collectable energy. Solar Energy 61(3): 191-201.
[11] Siala, F. M. F. and Hooper, F. C. (1990). A model for the directional distribution of the diffuse sky radiance with an application to a CPC collector. Solar Energy 44(5): 291-296.
[12] Igawa, N., Koga, Y., et al. (2004). Models of sky radiance distribution and sky luminance distribution. Solar Energy 77(2): 137-157.
[13] Perez, R., Seals, R., et al. (1993). All-weather model for sky luminance distribution - Preliminary configuration and validation. Solar Energy 50(3): 235-245.
[14] Badescu, V. (2008). Modeling Solar Radiation at the Earth's Surface: Recent Advances. Berlin, Springer Verlag.
[15] Remund, J., Müller, S., et al. (2007). Meteonorm: Global Meteorological Database, Part 1: Software, Version 7. Bern, Meteotest.
[16] Perez, R., Seals, R., et al. (1987). A new simplified version of the perez diffuse irradiance model for tilted surfaces. Solar Energy 39(3): 221-231.
[17] Klein, S. A., Beckman, W. A., et al. (2012). Trnsys 17 - a TRaNsient SYstem Simulation program. Programmer´s Guide, Solar Energy Laboratory, University of Wisconsin-Madison.
[18] Brandemuehl, M. J. and Beckman, W. A. (1980). Transmission of diffuse radiation through CPC and flat plate collector glazings. Solar Energy 24(5): 511-513.
[19] Carvalho, M. J., Horta, P., et al. (2007). Incidence angle modifiers: A general approach for energy calculations. ISES Solar World Congress.